Journal of Rock Mechanics and Geotechnical Engineering 5 (2013) 1–17

Contents lists available at SciVerse ScienceDirect

Journal of Rock Mechanics and Geotechnical Engineering

journal homepage: www.rockgeotech.org

Analysis of hydro-mechanical processes in a ventilated tunnel in an argillaceous rock on the basis of different modelling approaches

B. Garitte[a,*], A. Bond[b], A. Millard[c], C. Zhang[d], C. Mcdermott[e], S. Nakama[f], A. Gens[a]

[a] Universidad Politécnica de Catalunya, Barcelona, Spain
[b] Quintessa, Warrington, UK
[c] Commissariat à l'Energie Atomique, Gif-sur-Yvette, France
[d] Chinese Academy of Sciences, Wuhan, China
[e] ECOSSE, University of Edinburgh, Edinburgh, UK
[f] Japan Atomic Energy Agency, Tokai, Japan

ARTICLE INFO

Article history:
Received 1 April 2012
Received in revised form
10 September 2012
Accepted 15 September 2012

Keywords:
Hydro-mechanical (HM) coupling
Numerical modelling
Mont Terri Underground Rock Laboratory (URL)
Ventilation experiment (VE)
Argillite
Water permeability

ABSTRACT

In this paper, a modelling benchmark exercise from the DECOVALEX-2011 project is presented. The benchmark is based on the performance and results of a laboratory drying test and of the ventilation experiment (VE) carried out in the Mont Terri Underground Rock Laboratory (URL). Both tests involve Opalinus clay. The work aims at the identification, understanding and quantification of mechanisms taking place during the ventilation of a gallery in argillaceous host rocks on one hand and at investigating the capacity of different codes and individuals to reproduce these processes on the other hand. The 4-year in situ VE took place in a 1.3 m diameter unlined tunnel and included two resaturation–desaturation cycles. The test area was equipped with over one hundred sensors (including the global water mass balance of the system, relative humidity (RH), water content, liquid pressure, relative displacement and concentration of some chemical species) to monitor the rock behaviour during ventilation. The laboratory drying experiment, carried out before the VE, was designed to mimic the in situ conditions. The work was organized in a progressive manner in terms of complexity of the computations to be performed, geared towards the full hydro-mechano-chemical (HMC) understanding of the VE, the final objective. The main results from the modelling work reported herein are that the response of the host rock to ventilation in argillaceous rocks is mainly governed by hydraulic processes (advective Darcy flow and non-advective vapour diffusion) and that the hydro-mechanical (TM) back coupling is weak. A ventilation experiment may thus be regarded as a large scale-long time pump test and it is used to determine the hydraulic conductivity of the rock mass.

1. Introduction

During the construction and operation phases of a radioactive waste repository, the underground drifts will be subjected to a more or less intense ventilation period, which could produce partial desaturation of the rock around the drifts. Design of future storage facilities for radioactive waste in deep geological media requires a thorough understanding of the mechanisms occurring near the installations. This understanding is achieved by the parallel development of in situ tests, mimicking expected storage conditions such as mechanical loading, ventilation, heating, and theoretical thermo-hydro-mechanical-chemical (THMC) formulations. On one hand, the exploration of the THMC formulations allows the identification of possible processes involved near storage galleries. On the other hand, the analysis of in situ tests establishes the validity of the formulations based on the comparison of numerical results with data collected during the tests.

In order to investigate the effects of ventilation on Opalinus clay in the Mont Terri Underground Rock Laboratory (URL), a 10 m long section of an unlined microtunnel, 1.3 m in diameter, was sealed off in July 2002, and a ventilation system was installed in March 2003 (Mayor and Velasco, 2008). The microtunnel was raise-bored in February 1999. Between May and July 2002, the region 2 m in radius around the test section was instrumented with hygrometers, for measuring the relative humidity (RH),

* Corresponding author. Tel.: +34 677300898.
E-mail address: benoit.garitte@gmail.com (B. Garitte).

Peer review under responsibility of Institute of Rock and Soil Mechanics, Chinese Academy of Sciences.

Production and hosting by Elsevier

1674-7755 © 2013 Production and hosting by Elsevier B.V. on behalf of Institute of Rock and Soil Mechanics, Chinese Academy of Sciences.
http://dx.doi.org/10.1016/j.jrmge.2012.09.001

piezometers and extensometers. The RH is defined as the ratio of the partial pressure of water vapour in the mixture to the saturated vapour pressure of water at a given temperature. Several drilling campaigns were also run at different stages of the experiment to estimate the distribution of water content and chloride and sulphate concentrations around the microtunnel.

The VE was carried out in two phases. In the first phase, the VE tunnel was subjected to resaturation (11 months, starting from July 2002), then dry air was ventilated through the test section (8 months). In the second phase, a second resaturation and desaturation cycle was applied (11.5 and 20.5 months, respectively). The VE ended in September 2006. The significance of the study lies in the fact that all drifts and tunnels in the repository will be subjected to ventilation effects to some extent during the operative phase of the facility. In realistic operation scenarios, RH is estimated to be 60%–90% (Meier, 1998, 2004; Gisi, 2007). During the drying cycles of the VE, the RH of incoming air varied between 2% and 30% to ensure stronger drying conditions over a limited period of time. It is believed that argillaceous rocks may be especially sensitive to the actions of this type. Specifically, the following issues are potentially involved:

(1) Desaturation/resaturation of the rock, and phase changes;
(2) Air/rock interface;
(3) Damage/microcracking of the host rock due to hydro-mechanical and/or chemical effects;
(4) Evolution of the excavation damaged zone (EDZ).

The DECOVALEX project (acronym for DEvelopment of COupled models and their VAlidation against EXperiments) was set up to support the development of computer codes and to compare model calculations with results from field and laboratory experiments. In the latest phase of the project (2008–2011), one of the tasks consisted of the analysis of the VE. In this paper, the general layout of the task and the main results are described:

(1) The identification of relevant processes and of Opalinus clay parameters on the basis of the laboratory drying test.
(2) Simple hydro-mechanical modelling of the VE up to the end of the first drying phase on the basis of the laboratory parameters and calibration of the models.
(3) Advanced hydro-mechanical modelling of the VE, including blind prediction of the second drying period.

Specific issues linked to the task were treated in companion papers. One of the main difficulties experienced in the modelling exercises was the treatment of the evaporation boundary condition at rock–air interface. Bond et al. (2013a) reported the advances made by the different teams in that aspect. Millard et al. (2013) focused on the anisotropic nature of Opalinus clay and estimated the effects of anisotropic properties and stress state on the modelling results. The last companion paper (Bond et al., 2013b) described the chemical changes in argillaceous rocks resulting from ventilation and summarized the results obtained by the teams on conservative and reactive transport.

The participating modelling teams and the corresponding funding organizations are:

(1) CAS (Chinese Academy of Sciences, China);
(2) CEA (Commissariat à l'Energie Atomique) on behalf of IRSN (Institut de Radioprotection et de Sûreté Nucléaire, France);
(3) Quintessa on behalf of NDA (Nuclear Decommissioning Authority) (UK);

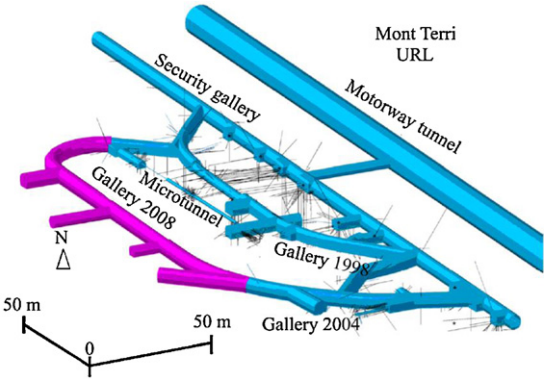

Fig. 1. 3D view of the Mont Terri URL.

(4) UoE (University of Edinburgh) on behalf of NDA (Nuclear Decommissioning Authority) (UK);
(5) JAEA (Japan Atomic Energy Agency, Japan).

2. Mont Terri and the ventilation experiment

The Mont Terri project started in 1995, as a collaboration between not less than eleven organizations from six different countries to investigate the hydrogeological, geochemical and geotechnical characteristics of an argillaceous rock formation (Opalinus clay). The project is based on the construction of a URL built as an extension of the security gallery of a highway tunnel between St-Ursanne and Courgenay in Switzerland (Fig. 1). Four main construction phases were carried out: in 1996, several niches were excavated from the security gallery; in 1998–1999, a first gallery and the microtunnel in which the VE took place were excavated; and in 2004 and 2008, two new extensions were bored, respectively. Scientific experiments were set up from the different niches and galleries to investigate the rock response to excavation, ventilation, heating and bentonite emplacement (Thury and Bossart, 1999).

2.1. Opalinus clay

Opalinus clay is a stiff over-consolidated clay of Lower Aalenian age, corresponding to the Middle Jurassic. It was found in the Jura Mountains of Northern Switzerland. Its mineralogy consists mainly of sheet silicates (illite, illite-smectite mixed layers, chlorites, kaolinites), framework silicates (albites, K-feldspar), carbonates (calcite, dolomite, ankerite and siderite) and quartz (Bossart et al., 2002). There are three slightly different facies containing different mineral proportions: a shaly facies in the lower part of the deposit, a 15 m thick sandy-silty facies in the centre and a sandy facies interstratified with shaly facies in the upper part. The content of clay minerals may range from 40% to 80%, depending on the facies. The clay is sedimented in marine conditions, and its pore water is highly mineralized with total dissolved solids up to 20 g/L. This water contains a significant amount of seawater millions of years old. Total thickness is about 160 m.

In the location of the Mont Terri laboratory, the overburden depth varies between 250 m and 320 m (it is estimated that overburden reached at least 1000 m in the past). The laboratory is situated in an asymmetrical anticline formed during the folding of the Jura Mountains as shown in the geological cross-section of Fig. 2. The rock strata dip, because of the tectonic activity, with an angle of 30°–45° to the southeast. The bedding trace is perpendicular to the axis of the motorway tunnel. A picture of an Opalinus

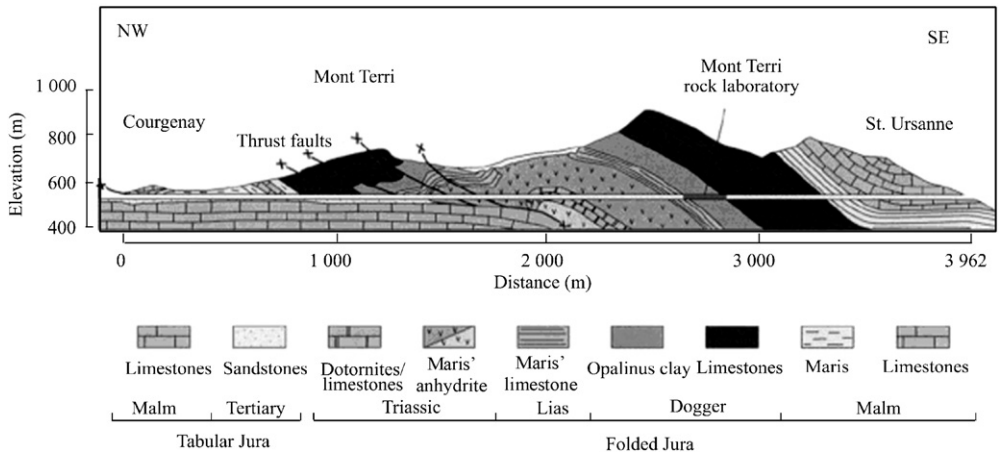

Fig. 2. Geological profile in the vicinity of the Mont Terri underground laboratory as a function of the motorway tunnel metres (Schaeren and Norbert, 1989; Thury and Bossart, 1999).

Fig. 3. Opalinus clay sample.

clay sample showing clearly the strong layering of the material is presented in Fig. 3.

Opalinus clay behaviour has been intensely studied by means of laboratory and in situ experimental programmes in the framework of the Mont Terri project. A general synthesis of the main physical and geotechnical parameters was reported in Bock (2001) and Wileveau (2005). Based on this information, the reference values of a series of parameters together with their likely ranges have been listed in Table 1. It can be noted that some of the parameters have different values depending on the orientation of the material, reflecting the anisotropy caused by the strong bedding of the clay.

When information is scarce, no range estimation has been quoted. The following additional remarks can be made:

(1) Reference elastic parameters have been based on measurements made in triaxial and uniaxial compression tests and on results of field dilatometer tests.
(2) The reference shear strength parameters have been derived from laboratory triaxial tests. As strength depends on water content, only strength data for which the moisture content was within the range of the natural water content were considered.
(3) Permeability measurements were made on laboratory specimens and using in situ boreholes. The dispersion of the in situ permeability measurements is illustrated in Fig. 4, as this parameter has an important influence on the results of the VE, which can be considered as a huge pump test itself.
(4) Biot's coefficient is uncertain due to limited data.

The reference values have been used as a basis for estimating the parameters required in the numerical analyses reported below. However, alternative values have been adopted if information referring more specifically to the location of the ventilation in situ test was available.

A significant number of measurements using different procedures (borehole slotter, undercoring, and hydraulic fracturing) of the in situ stress have been made. They have been supplemented by geological observations and back analysis of instrumented excavations. A synthesis of the information available is reported in

Table 1
Reference parameters for Opalinus clay (Wileveau, 2005).

Mineralogy			Petrophysical properties			Hydraulic and hydromechanical properties	
Clay content (%)	Carbonate content (%)	Quartz content (%)	Density, ρ (g/cm^3)	Water content, w (%)	Porosity, ϕ (%)	Water permeability of sound clay, k (m/s)	Biot's coefficient, b
62 (44–80)	14 (6–22)	18 (10–27)	2.45 (±0.03)	6.1 (±1.9)	15.7 (±2.2)	10^{-13} (10^{-12} to 10^{-14})	0.6 (0.42–0.78)

Mechanical properties											
Uniaxial compression strength (MPa)		Tensile strength (MPa)		Elastic modulus (MPa)		Poisson's ratio		Shear strength parameters			
$R_{c//}$	$R_{c\perp}$	$R_{t//}$	$R_{t\perp}$	$E_{//}$	$E_{\perp}$	$\nu_{\perp//}$	$\nu_{////}$	$c'_{//}$ (MPa)	$\varphi'_{//}$ (°)	$c'_{\perp}$ (MPa)	$\varphi'_{\perp}$ (°)
10 (±6)	16 (±6)	1	0.5	10,000 (±3700)	4000 (±1000)	0.24	0.33	2.2	25	5.0	25

Note: The symbols "//" and "⊥" refer to the material orientation parallel and perpendicular to the bedding, respectively. The data in brackets represent the range of the parameters.

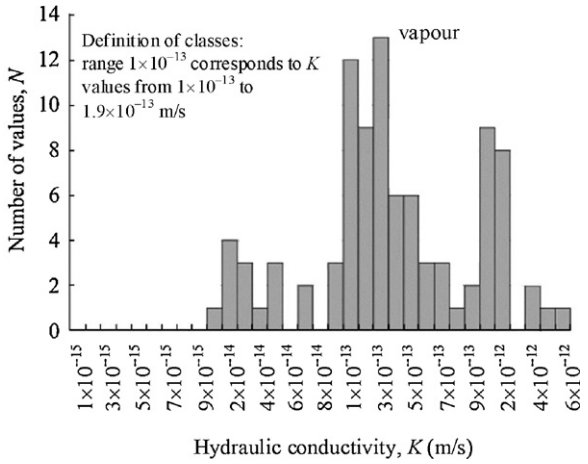

Fig. 4. Compilation of results from field permeability tests performed on Opalinus clay in the Mont Terri underground laboratory (Nussbaum and Bossart, 2004).

Wermeille and Bossart (1999) and in Martin and Lanyon (2003). The following comments can be made:

(1) The major principal stress is subvertical and corresponds approximately with overburden weight (about 7 MPa).
(2) The magnitude of the intermediate principal stress obtained from undercoring is consistent with the results from hydraulic fracture tests (about 5 MPa).
(3) The value of the minor principal stress is quite low (about 2 MPa) and probably controlled by the presence of a deep valley to the SW of the laboratory. A low value of the minor principal stress is consistent with the small number of breakouts observed in vertical boreholes.

2.2. Technical features of the VE

The VE has been performed in a 10 m long section of the unlined raise-bored microtunnel (1.3 m in diameter), excavated in 1999 in the shaly facies section. The VE section is presented in Fig. 5. Different vertical planes (SA*x*, SB*x*, SC*x* and SD*x*) were instrumented along the test section.

The VE was sealed off by means of two double doors made of exotic wood (wengé) insensitive to RH variations (Fig. 6). The controlled ventilation during the test was accomplished using a system consisting of a blowing device that was located outside the test section (by a compressor, a drier and a bubbler), and inflow and outflow pipes that were equipped with flowmeters and hygrometers. Measurement of airflow mass (q_g) and RH of in- and out-going

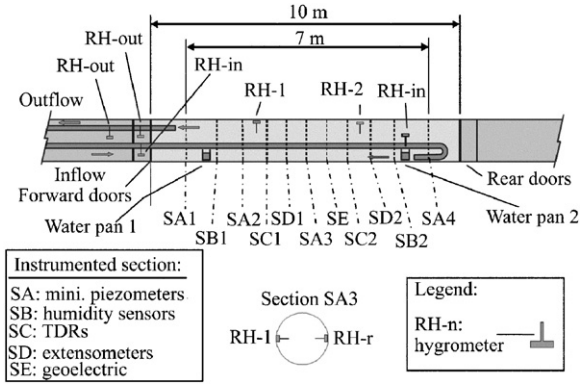

Fig. 5. Layout of the VE.

Fig. 6. Picture of the test section.

air allowed for establishing the global water mass balance of the test section according to

$$\theta_g^w = \omega_g^w \rho_g = \frac{RH}{100}\frac{p_{v0} M_w}{RT} \quad (1)$$

where θ_g^w is the volumetric mass of water in the gas phase, $\omega_g^w = m_w/m_g$ is the mass fraction of water in the gas phase, p_{v0} is the vapour pressure for saturated state, M_w is the molecular mass of water, R is the universal gas constant, T is the temperature, and ρ_g is the gas density (kg/m^3). The water mass flux q_w (kg/h) is written as

$$q_w = \theta_g^w q_g \quad (2)$$

The test history is illustrated in Fig. 7, in which the RH of the test section is plotted as a function of the time in the 12-year interval (149 months) between the excavation of the microtunnel and 2011. In this paper, we focus on the period between the excavation of the microtunnel and the end of the controlled ventilation. Several phases can be usefully distinguished:

(1) Phase 0, in which the VE tunnel was excavated and left open without controlled ventilation conditions (from February 1999 to July 2002). This phase lasted for about 3.5 years (41 months).
(2) Phase 1, in which the VE tunnel was subjected to controlled ventilation conditions resulting in rock resaturation (from July 8th 2002 to May 28th 2003) and subsequent desaturation (from May 28th 2003 to January 29th 2004). This phase lasted for about 1.5 years (19 months).

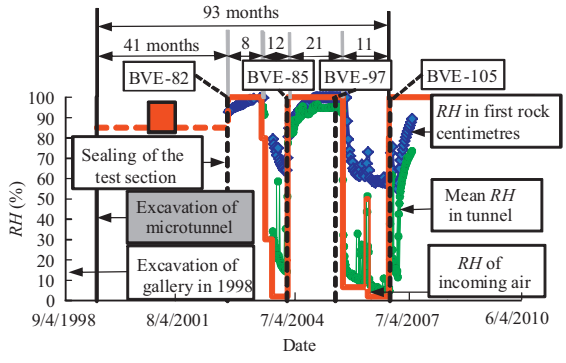

Fig. 7. Relative humidity history of the test section.

(3) Phase 2, in which an additional episode of controlled resaturation (from January 29th 2004 to July 11th 2005) and desaturation (from July 11th 2005 to September 24th 2006) was performed. This phase lasted for about 2.5 years (33 months).

Finally, a last resaturation stage was applied.

In Phase 0, representative of natural ventilation of a niche (tunnel is closed at one end), the RH in the tunnel was not measured. Nevertheless, some relative humidity measurements are available at several locations in the URL. Meier (1998) measured the RH in gallery and came up with values around 50%. Meier (2004) and Gisi (2007) measured the RH in boreholes. They monitored values of 80%–90% and 75%–95%, respectively. As the microtunnel is closed at one end, its configuration is similar to that of a borehole. Moreover, Garitte and Gens (2011) back calculated the value of the RH in the tunnel (85%) in this period to reproduce correctly the pore water pressure and the water content gradient around the tunnel before the controlled ventilation period.

Phase 1 corresponds with the VE itself and starts with the sealing of the test section with two double doors. Only by isolating the section, the measured RH in the tunnel approaches 100%. The RH in the first rock centimetres increases progressively. After 11 months, the rock mass is believed to be saturated and the first drying phase starts. RH of blown air is as low as 2% and that in the tunnel decreases down to 15%. In the first rock centimetres, RH decreases to 65%. The resaturation–desaturation process is then repeated in Phase 2.

Several drilling campaigns were carried out at key moments to obtain radial profiles of water content and chloride and sulphate concentrations:

(1) Borehole BVE-82 on July 5, 2002 before isolation of the test section.
(2) Boreholes BVE-85 and BVE-86 on January 26, 2004 at the end of the first desaturation.
(3) Boreholes BVE-97, BVE-99 and BVE-100 on May 1, 2005 at the end of second resaturation.
(4) Boreholes BVE-105, BVE-106, BVE-107, BVE-109 and BVE-110 on October 4, 2006 at the end of the second desaturation.

Table 2
Summary of the emplaced sensors.

Measurement item	Sensors (boreholes) number	Min. and max. distance to tunnel wall (m)
RH measurement in the tunnel	10	Up to 0.02
Water evaporation in water pans	2	–
RH measurements in the rock mass	24	0.25 (0.07)–1.5
Water balance of the system	–	–
Water content profiles	13	0–1 (1.5)
Chloride and sulphate concentration profile		
Water pressure evolution	28	0.5–1.5 (5.6)
Relative displacements	8	Between wall and 2 m inside

Note: Before Phase 2, new instrumentation was emplaced extending the instrumented range. The new range is indicated by the values between brackets.

The time of the drilling campaign is indicated in Fig. 7 by vertical dotted lines. The information from borehole BVE-82 and from the piezometers installed at that time was used to back calculate the most likely value of RH in the microtunnel between its excavation and the sealing off of the test section. The instrumentation system installed in the VE area is summarized in Table 2.

Different geophysical methods (seismic refraction, interval velocity and cross-hole measurements) were applied to evaluate the extent and the development of the EDZ around the microtunnel (Schuster, 2007). The extent of the EDZ was estimated to be 5–25 cm in the bedding planes direction and 10 cm in the perpendicular direction. No significant changes induced by ventilation were identified and the EDZ was thus related to stress redistribution during the excavation exclusively. Moreover, observation of the tunnel wall showed that the state of the rock surface in the test section before and after the two drying phases was fairly good: neither relevant rock failures nor far-reaching cracking were observed on the walls (Mayor and Velasco, 2008). The small displacements registered in the extensometers during the different cycles tend to confirm the fact that the EDZ does not develop during drying and wetting. Garitte and Gens (2011) predicted an extent of the EDZ (by modelling) of about 30 cm. According to this modelling, the EDZ was intensified during the ventilation cycles but not extended significantly.

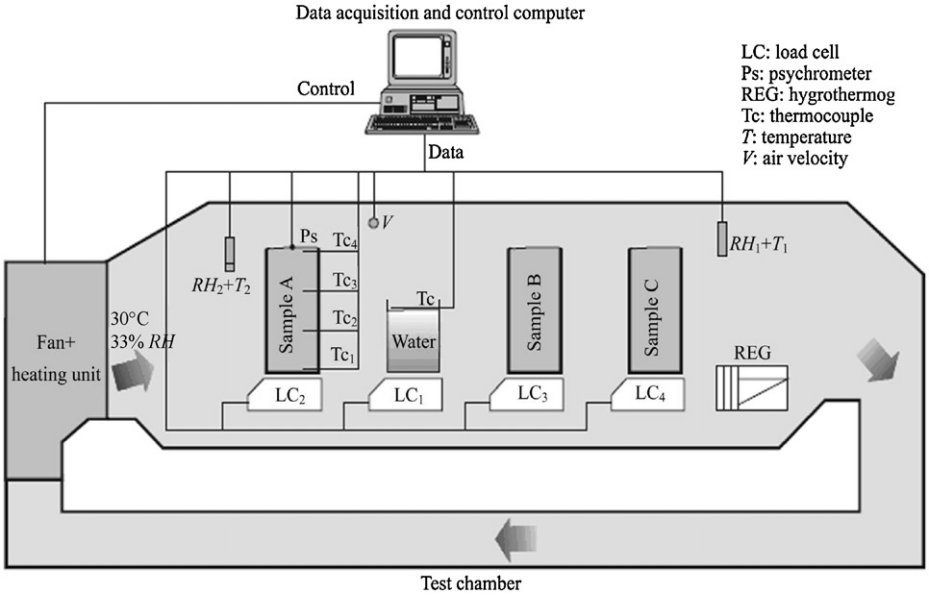

Fig. 8. Layout of the laboratory drying test.

The laboratory drying test (Floría et al., 2002) was performed in 2001, before the start of the in situ VE. Three cylindrical Opalinus clay samples (0.28 m in height and 0.1 m in diameter) and a water pan were placed on balances in a drying chamber. The layout of the laboratory drying test is presented in Fig. 8.

All sample walls, except the top, were isolated in order to create conditions as close as possible to one-dimensional (1D) flow. The atmospheric conditions applied through a fan and heating unit were measured in various sensors inside the chamber. The values of RH (measured on top of the samples) varied between 20% and 50%. A constant temperature of 30 °C was maintained. The air velocity applied was between 30 cm/s and 70 cm/s. The evaporation rate and water loss from a water pan were also measured to act as a reference.

Continuous weight measurement allowed a direct estimation of the water loss in each of the samples. A perhaps fortuitous correlation should be noted: the sample closest to the fan heating unit loses most water and the farthest one the least. After 142 days of testing, sample A had lost about 150 g from the initial 352 g. Complementary information about the water content distribution was obtained at 21 and 99 days by withdrawing a sample at each of those times, cutting it into 3 cm slices and measuring the water content of each slice. Integrating the water content profiles, we found a water loss of 59 g, 121 g and 151 g for samples C, B and A, respectively. That corresponds remarkably well with the water loss obtained through the continuous weight measurements, which increases the confidence in the experiment.

3. Theoretical formulations and participants

Only a summary of the different formulations used by the teams is reported herein. The different equations resolved by the teams and their corresponding codes are given in Table 3. Most of the codes, FRT-THM, CAST3M (Verpeaux et al., 1989), THAMES (Chijimatsu et al., 1998) and RockFlow/Geosys are finite element codes and only QPAC (Maul, 2010), the code used by Quintessa, is a finite volume code. There was a common agreement that the water mass balance was the most important equation by far. Air mass and energy balances were found to have a negligible influence as the gas pressure and the temperature were constant throughout the test. Deformation of the porous medium (stress equilibrium) affects the water mass balance, but its effects may be categorized as second order (Millard et al., 2013). Solute transport and reactive transport were affected by the desaturation of the rock mass around the microtunnel, but the back coupling was estimated to be negligible (Bond et al., 2013b).

3.1. Common basis

The previous considerations lead us to focus on the equation of the water mass balance:

$$\frac{\partial}{\partial t}(\theta_l^w S_l \phi + \theta_g^w S_g \phi) + \nabla \cdot (j_l^w + j_g^w) = f^w \tag{3}$$

where ϕ is the porosity, θ_l^w is the volumetric masses of water in the liquid phase; S_l and S_g are the degrees of saturation of liquid and gas phases, respectively; j_l^w and j_g^w are the mass fluxes of water in the liquid and gas phases, respectively; $\theta_l^w = \omega_l^w \rho_l$, where $\omega_l^w = m_w/m_l$ is the mass fraction of water in the liquid, and ρ_l is the density of liquid.

We distinguish the changes of water mass in a certain volume due to changes in porosity, degree of saturation, and liquid and gas densities with respect to time in the first term and the divergence of water fluxes in the second term. The third term is a sink/source term which is equal to 0 in the present problem.

The advective flow of water in the liquid phase j_l^w (kg/m^2 s) is

$$j_l^w = \theta_l^w q_l \tag{4}$$

where q_1 is the Darcy velocity (m/s), i.e. the volumetric flow/section, which is proportional to the water pressure gradient ∇P_l (Pa/m):

$$q_l = -\frac{k k_{rl}}{\mu_l} \nabla P_l \tag{5}$$

where k is the intrinsic permeability (m^2), μ_1 is the dynamic viscosity (Pa s), and k_{rl} is a coefficient depending on the degree of saturation.

The dependence of the permeability on the degree of saturation is introduced through

$$k_{rl} = \sqrt{S_l}\left[1 - \left(1 - S_l^{1/\lambda'}\right)^{\lambda'}\right]^2 \tag{6}$$

known as Van Genuchten law, where λ' is a shape parameter. The transport of water in the gas phase can be decomposed into

$$j_g^w = (i_g^w)_{advection} + (i_g^w)_{diffusion} + (i_g^w)_{dispersion} \tag{7}$$

where the first term in the right represents the flux of water by motion of the gas phase and the second term in the right the flux of water by diffusion of water vapour inside the gas phase (non-advective flow). Dispersion was neglected. Gas motion was found to be negligible as gas pressure is constant throughout the test. Vapour diffusion is expressed by Fick's law:

$$(i_g^w)_{diffusion} = -(\phi \rho_g S_g D_g^w \boldsymbol{I}) \nabla \omega_g^w \tag{8}$$

where D_g^w is the vapour diffusion coefficient (m^2/s); and $\nabla \omega_g^w$ is the gradient of vapour concentration, defined as the ratio of the mass of water in the air to the mass of air. Vapour diffusion was found to have a significant influence on the results. The relationship between suction ($P_g - P_l$) and the liquid degree of saturation is idealized by the modified Van Genuchten retention curve:

$$S_e = \frac{S_l - S_{rl}}{S_{ls} - S_{rl}} = \left[1 + \left(\frac{P_g - P_l}{P}\right)^{(1/(1-\lambda))}\right]^{-\lambda} \left(1 - \frac{P_g - P_l}{P_s}\right)^{\lambda_s} \tag{9}$$

where λ is a shape parameter, S_{rl} is the residual saturation, S_{ls} is the maximum saturation; P_s and λ_s are two material parameters, and P corresponds with the air entry value.

For suction values lower than the air entry value, water is retained in the clay pores although the pore water is submitted to tension. When suction exceeds the air entry value, the porous material starts to desaturate. This allows the distinction between

Table 3
Summary of the codes and balance equations used by the modelling teams.

Team	Code	Water balance	Solid balance	Air mass balance	Energy balance	Stress equilibrium	Solute transport	Reactive transport
CAS	FRT-THM	X	X	X	X	X	X	
CEA	CAST3M	X	X			X	X	
JAEA	THAMES	X	X		X	X	X	
Quint.	QPAC	X	X	X	X	X	X	X
UoE	RocFlow/Geosys	X	X	X			X	

a suction limit and a desaturation limit. UoE used another relationship (Ippisch et al., 2006). Finally, we make the hypothesis that water in the pores, in vapour form and in liquid form, is in equilibrium, through Kelvin's law that relates water content in the gas phase to the suction in the liquid phase:

$$\theta_g^w = \omega_g^w \rho_g = (\theta_l^w)^0 \exp\left[\frac{-(P_g - P_l)M_w}{(273.15+T)R\rho_l}\right] \quad (10)$$

The relative humidity can be related to θ_g^w through

$$RH = \frac{p_v}{(p_v)_0} \times 100\% = \frac{\theta_g^w}{(\theta_g^w)_0} \times 100\% \quad (11)$$

where p_v is the vapour pressure, and subscript $(\cdot)_0$ stands for saturated state.

3.2. Conceptual models and specific features

A considerable amount of computation was run by the different teams for the laboratory drying test and for the VE. In both cases, 1D, 2D (two-dimensional) and 3D (three-dimensional) models were developed.

For the laboratory drying test, the first modelling iteration round showed that the 1D hypothesis was appropriate enough to tackle the case. The samples were considered as being initially saturated (7.14% of water content) and in equilibrium with the atmospheric pressure (pore water pressure and total stresses of 100 kPa). For the in situ VE, 1D modelling was shown to provide satisfactory results. In this case, the tunnel wall was considered as a boundary condition. Obviously, treatment of the anisotropy required an upgrade of the model to 2D (plane strain). Improved treatment of the evaporation boundary condition, in which the in- and out-pipes were considered as model boundary and the air flow in the tunnel was modelled (Bond et al., 2013a), implied the development of 3D models. The initial conditions considered a water pressure of 1.85 and 2.0 MPa and a stress state of 4.5 MPa, both representative of the situation at Mont Terri (Gens et al., 2007). The excavation and history of the microtunnel were simulated.

VEs are intended to investigate how an initially saturated porous medium dries when submitted to a dry environment. A key issue related to that is the exchange of water between the rock and the dry environment. In this kind of low porosity material, water is believed to leave the rock as vapour. Evaporation, the process by which molecules in a liquid state spontaneously become gaseous, occurs at rock–air interface and in the desaturated porous material near the evaporation boundary. Hereby the relative humidity profile, a measurement of the amount of water vapour that exists in a gaseous mixture of air and water, may be continuous along the rock–air interface or discontinuous as a consequence of the nature of the interface, the wind velocity in the tunnel and the water availability in the rock (that depends on the pore size, pore distribution and the degree of saturation of the interface pores). Although the evaporation boundary condition has been treated in detail in Bond et al. (2013a), a summary is given here.

The water loss from the pans and the samples in the laboratory drying experiment is used to discuss the evaporation boundary condition (Fig. 9). The water loss from the pans acts as a reference for free surface evaporation. At 20, 100 and 140 days, we know the measured degree of saturation on top of the samples as at each of these times one sample has been taken out of the chamber. The equivalent free water surface on top of the sample may be estimated by multiplying the top area with the porosity and the degree of saturation. Multiplying the water loss from the pans by that factor, we obtain an equivalent water loss that may be compared to the water loss from the samples (triangular symbols in Fig. 9). This

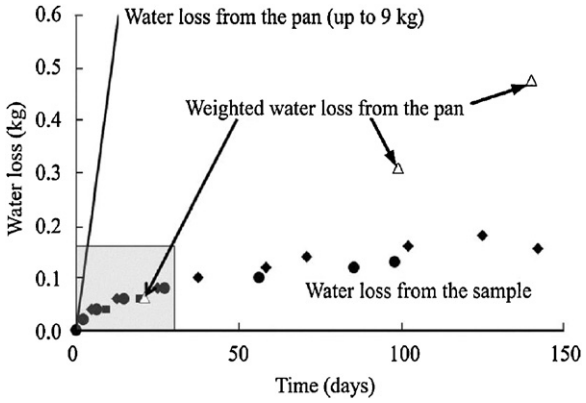

Fig. 9. Measured water loss in the laboratory drying test: from the water pan and the samples.

comparison seems to indicate that (at least) in the first 20 days of the experiment, the water on top of the sample behaves as free surface water. Later on a clear deviation from that behaviour is observed. This deviation reflects the imperfectness of the air–rock interface.

The numerical treatment of the evaporation boundary condition was done using three different approaches. The most straightforward is to apply directly the measured relative humidity (on top of the sample or on the tunnel wall):

$$RH_{boundary} = RH_{measured} \quad (12)$$

According to the water loss measurements in the laboratory experiment (Fig. 9), this option is only adequate for the first days of the experiment when the sample is almost saturated. Nevertheless, different computations have shown that using this option for the entire duration of the laboratory experiment does not induce a significant error. For the in situ ventilation instead, applying directly the relative humidity was shown to provide unsatisfactory results. The teams using this option had to apply a RH value between the RH measured in the tunnel and that measured in the first rock centimetres. JAEA, for instance, determined an empirical relationship between RH in the gallery and RH to be applied.

The second option consists in applying a water vapour flux as

$$j_g^w = \beta_g[(\rho_g \omega_g^w)^0 - (\rho_g \omega_g^w)] \quad (13)$$

where the superscript $(\cdot)^0$ stands for the prescribed values, and β_g is a penalty or interface coefficient (m/s) that controls the velocity at which the contour values tend to the prescribed values. For low β_g values, equilibrium is not reached instantaneously and less water is extracted. For high β_g values, Eq. (13) degrades to Eq. (12). The penalty coefficient may depend on degree of saturation and/or porosity of the interface elements. This allows for having high values when the rock surface is saturated and low values when water availability is low. Constant β_g values were shown to be sufficient to reproduce correctly RH in the first rock centimetres applying RH measured in the tunnel.

It was shown that using Eq. (13), it was possible to tackle the interface problem in a satisfactory way, but the observations of RH in the tunnel during the VE had to be used. Quintessa and CAS (Bond et al., 2013a) succeeded in developing an innovative approach (Option 3), consisting in modelling the tunnel air flow and the rock mass, and the boundary condition being displaced from the tunnel wall to the in-pipe. Prescribing the incoming air flow and its RH, they succeeded to predict the value of RH in the tunnel, in the first rock centimetres, the rock behaviour and RH of the out-coming air at the out pipe.

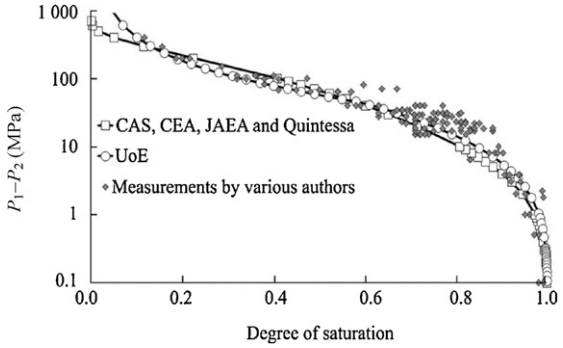

Fig. 10. Retention curves of Opalinus clay: measurements by various authors (Gens, 2000; Muñoz et al., 2003; Zhang and Rothfuchs, 2005; Villar, 2007) compared with the functions used by the different modellers.

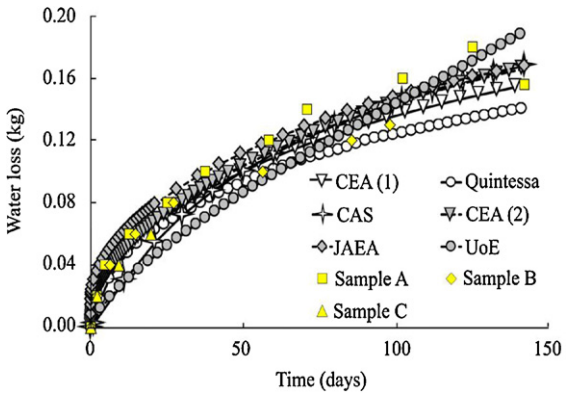

Fig. 11. Measurement and simulation of the water loss history.

In this section, we outlined the difficulties of the evaporation boundary condition and solutions employed to treat the problem. Evaporation does not occur only at the rock–air interface, but also in the desaturated ring around the microtunnel. In that zone, water transport occurs by (1) advection (Darcy's law) and (2) non-advective vapour diffusion. Vapour diffusion was only considered by CAS, CEA and Quintessa. JAEA, UoE and an additional computation by CEA(2) neglected vapour diffusion. The difference between the two approaches resulted in consistent differences in modelling results and parameters determination. Note that the vapour concentration gradient drives water vapour towards the air–rock interface and contributes to the water vapour amount available for leaving the rock.

4. Modelling results

4.1. Laboratory drying test

The modelling work started with the laboratory drying test because of its similarity with the VE in situ test and of its simple configuration. This test allowed for evaluating the capabilities of the different codes and the relative importance of the processes in place. In the first modelling iteration, most of the input parameters were taken from Table 1, although some of them had to be updated according to data specific to the test area. In the second modelling iteration, some of the parameters were calibrated. Sensitivity analyses have been presented in Garitte et al. (2009, 2010). These simulations showed the importance of: (1) the value of water permeability and its dependency on saturation, and (2) water transport through vapour diffusion. Point 1 was used to calibrate the model. The first step of the calibration consists in fitting the first days of the experiment to obtain the saturated permeability. The remaining time of the experiment is then used to calibrate the dependency of permeability on degree of saturation.

Physical properties (porosity, density, water content, etc.) were taken directly from reports describing the results of the VE drilling campaigns (Traber, 2003, 2004; Fernández et al., 2006). Measurements of water retention curves from four independent laboratories were used (Gens, 2000; Muñoz et al., 2003; Zhang and Rothfuchs, 2005; Villar, 2007) as an input for the models (Fig. 10). The retention curve was shown to have a significant influence on the results.

Comparison of the modelling results with the laboratory measurements has been organized in two groups: (1) the teams considering water transport through advective flux of liquid water and diffusion of water vapour (CAS, CEA(1) and Quintessa), and (2) the teams considering only advective flux as water transport mode (CEA(2), JAEA and UoE). Comparison of the water loss throughout the experiment is presented in Fig. 11. Simulation results produced by five different codes, based on independent parameters determination, lie within the measured variation range which is an achievement in itself.

The water content profiles at 21, 99 and 142 days are presented in Figs. 12 and 13, for CEA(2), JAEA and UoE and for CAS, CEA(1) and Quintessa, respectively. Both groups achieved not only quite a good agreement with the measurements, but also between themselves. For instance, the parameters sets used by CEA(2) and JAEA are very similar and this is reflected in the similarity of their modelling results. Further, we observe a good consistency between the continuous water loss results and water content profiles. For example, Quintessa's water loss results are in perfect agreement with the measurements from sample B that was retrieved from the chamber after 99 days, but overestimates sample C and underestimates sample A. The same tendency is observed in the water content profiles.

The dependency of water permeability on degree of saturation used by the different teams is illustrated in Fig. 14. Clearly, we observe two tendencies. CAS, CEA(1) and Quintessa (the teams considering vapour diffusion) had to use a relatively high saturated permeability value that decreases fast with decreasing saturation. That is because in the desaturated zone, part of the water transport occurs by vapour diffusion.

The relative importance of water diffusion and advective transport is illustrated in Fig. 15, representing simulated profiles of vapour to liquid flux ratio at different times. In the first days of the experiment, water transport occurs only through advection of liquid water. At this stage, water permeability used by the groups considering vapour diffusion is high and allows reproducing well the initially fast water loss. However, water transport quickly becomes dominated by vapour diffusion in the top centimetres of the sample as this zone desaturates. At the end of the test, the desaturation front reaches the bottom of the sample where the ratio grows up to 50%. The parameter sets determined by the different teams are summarized in Table 4.

In Fig. 16, the hydraulic conductivity values determined by the different teams on the basis of the laboratory drying test are compared to the geometric mean and the range of all the in situ measurements made in Mont Terri (Fig. 4) and to the pulse test measurements made in the piezometers of the VE (Mayor and Velasco, 2008). It is remarkable that the teams considering vapour diffusion have come up with values very close to the ones measured in the VE site. Hydraulic conductivity measurements in the VE test site are situated in the higher range in Mont Terri. Note that there is no clear indication of increasing permeability towards the tunnel, which may have been the case if an important

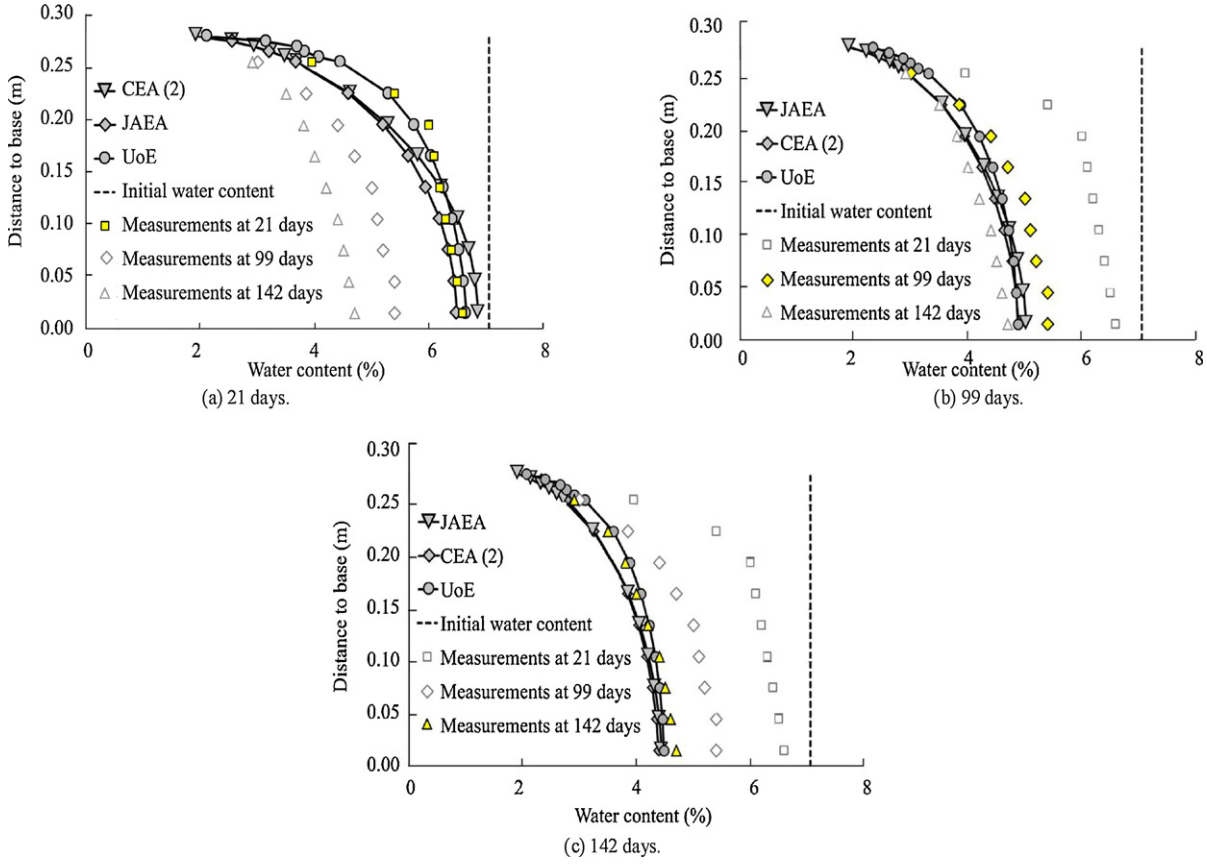

Fig. 12. Comparison of measured and simulated water content profiles in the sample taken out at various days for the teams that did not consider vapour transport.

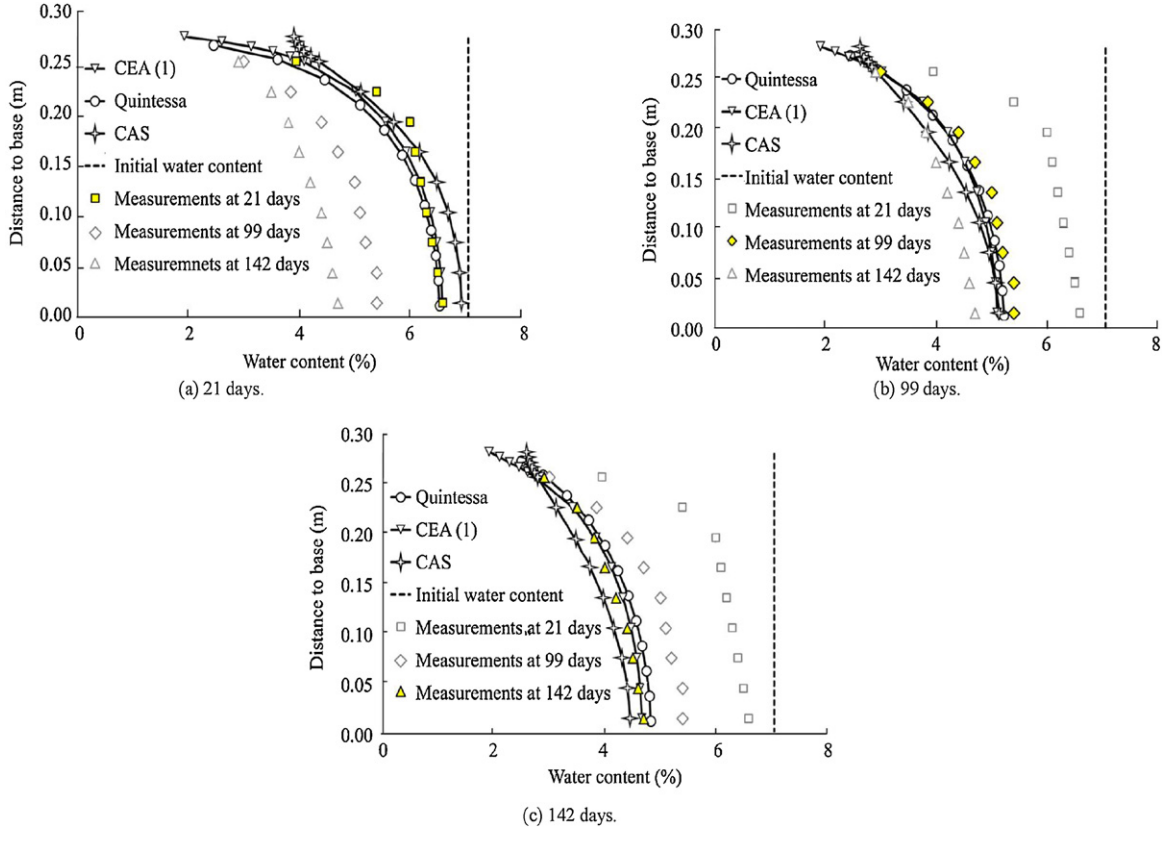

Fig. 13. Comparison of measured and simulated water content profiles in the sample taken out at various days for the teams that did consider vapour transport.

Table 4
Summary of the relevant parameters used by the different teams.

Team	Solid grain density, ρ_s (kg/m^3)	Porosity, ϕ	Intrinsic permeability, k (m^2)	Dynamic viscosity, μ (Pa s)	Liquid relative permeability, λ'	Vapour diffusion coefficient, D_g^w (m^2/s)
CAS	2710	0.165	7.5×10^{-20}	1×10^{-3}	0.4	6×10^{-6}
CEA(1)	2710	0.16	1×10^{-19}	8×10^{-4}	0.4	2.6×10^{-5}
CEA(2)	2710	0.16	2×10^{-20}	8×10^{-4}	0.68	
JAEA	2743	0.162	2×10^{-20}		0.65	
Quint.	2700	0.16	1.7×10^{-19}		0.3	5×10^{-6}
UoE		0.19	3.2×10^{-20}	1×10^{-3}	0.6	

Team	Young modulus, E (GPa)	Poisson's ratio, ν	Air entry value (RC), P_0 (MPa)	Shape parameter (RC), λ	Maximum suction (RC), P_s (MPa)	2nd shape parameter (RC), λ_s
CAS	6	0.27	3.9	0.128	700	2.73
CEA(1)	6	0.27	3.9	0.128	700	2.73
CEA(2)	6	0.27	3.9	0.128	700	2.73
JAEA			8	0.15	700	2.73
Quint.	2.5	0.3	3.9	0.128	700	2.73
UoE			3.9	0.44	[a]	3.6×10^{-8} [a]

[a] UoE used a different equation for the water retention curve (Brooks and Corey, 1966).

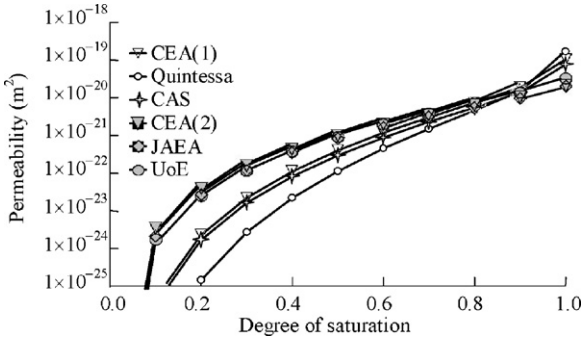

Fig. 14. Water permeability in function of the degree of saturation as used by the different teams.

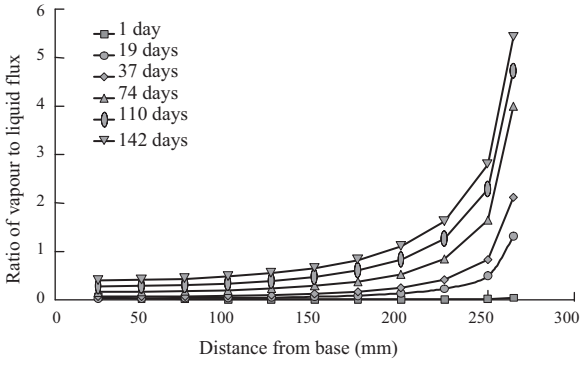

Fig. 15. Profiles of vapour to liquid flux ratio at different times (calculated by Quintessa).

EDZ is presented. A constant saturated water permeability was thus adopted as a starting point for the modelling of the VE.

4.2. VE modelling on the basis of laboratory determined parameters

The information collected in the analysis of the laboratory drying test was injected in the modelling of the in situ VE to assess the predictive capacities. At this stage, the teams were asked to compare their modelling results using the parameters determined in the laboratory drying test with the measurements from the first ventilation phase. The modelling results from the different teams may be considered as a benchmark between the teams as well

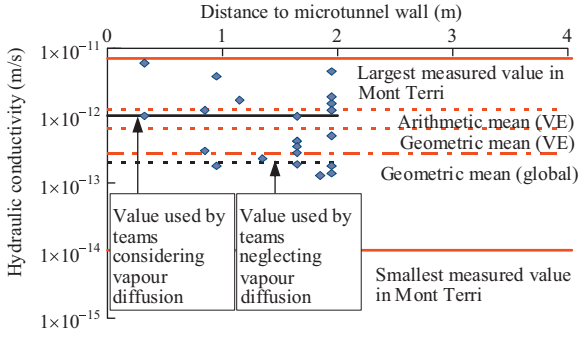

Fig. 16. Hydraulic conductivity values measured in the piezometers of the VE before the experiment (Mayor and Velasco, 2008). The geometric mean from all in situ measurements (Nussbaum and Bossart, 2004) was added.

as a validation exercise of the models against the measurements. After this first step, the models were calibrated in function of the measurements from Phase 1 and a sensitivity analysis was run to evaluate the current formulations capacities and seek for possible explanation for discrepancies between models and measurements. New elements were introduced and the acquired expertise was used to make a blind prediction of Phase 2, as described in the next section.

Pore water pressure, water content and relative humidity measured just before sealing the test section are plotted as a function of the distance to the tunnel axis in Fig. 17. The red straight line corresponds to the atmospheric pressure. Below this value, the pore water is likely to be in suction and the piezometers will cavitate (not lower pressure will be measured). The modelling results from the teams are added. According to the water content measurements, the partial desaturation limit lies between 13 and 31 cm from the wall. Behind 31 cm, the variation of water content is probably associated with measurements scatter. This trend is confirmed by the RH measurements that show a scatter between 95% and 100% behind 31 cm. 95% was estimated to be the in other galleries. The computation results from the teams provide quite a good agreement with the measurements considering the predictive nature of the exercise. The relatively good distinction between the partial desaturation limit and the suction limit reproduced by the models should be highlighted, although that achievement is strongly related to the care yielded to the calibration of the retention curve (Fig. 10).

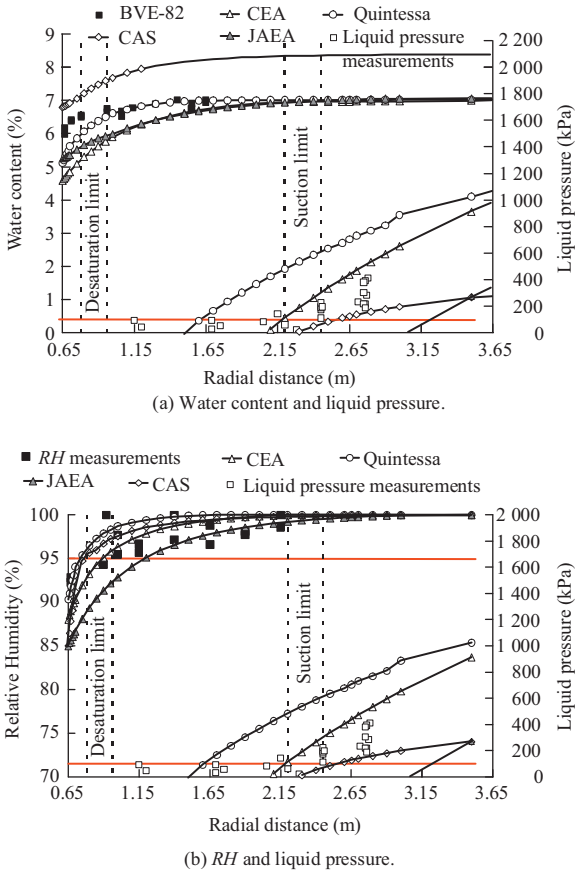

Fig. 17. Measured and simulated profiles of water content (BE-82) for RH and pore water pressure just before the sealing of the test section (5 July 2002).

Measurement of the global water mass balance of the in situ experiment is probably one of the main achievements of the VE as back calculation allows us to consider the experiment as a pump test involving an important volume of rock over a large duration. Indeed, in situ measurement of water permeability in low permeability porous medium is still a challenging issue as the technical problems encountered in conventional small scale-short duration pulse (or shut in) tests are not entirely resolved: injection of very small quantities of water, contact between the porous material and the injection chamber, and the volume contrast between the injection chamber itself and the pore volume. In the case of the VE, back calculation of the water permeability is obviously influenced by the estimation of the relative permeability and the water vapour diffusion in the partially desaturated zone and by advective water transport in the zone in suction where the validity of Darcy's law may be questioned.

The measured water mass balance and the modelling results are compared in Fig. 18. In this figure and in most other time evolution figures in this paper, the left hand scale represents the variable we are studying and the right hand scale represents the RH of incoming air to act as a time reference. Most of the teams reached a good agreement with the measurements. The prediction made by CEA should be highlighted: the agreement with the measurements was perfect. Their modelling results covered the measurement points. Direct application of the RH on the tunnel wall (Option 1 in Section 1), used by CAS and JAEA, seemed to produce an abrupt response to ventilation regime changes. This effect appeared to be attenuated by the use of a flux condition and a penalty coefficient (by CEA and Quintessa).

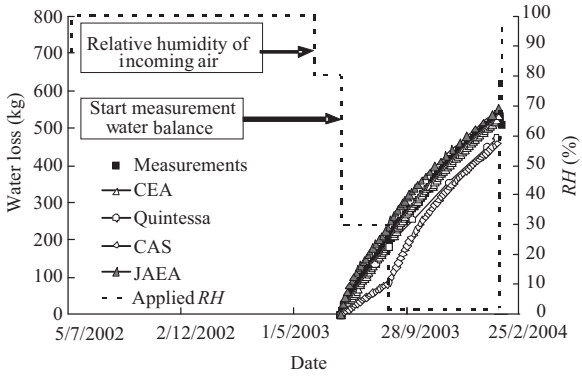

Fig. 18. Measured and simulated water mass balance of the test section.

The RH measured in the tunnel is presented in Fig. 19(a). The RH calculated by the teams on the tunnel wall is added. For JAEA this coincides with the applied RH which is the RH of the incoming air (Option 1). CAS applied a RH somewhat higher than that of the incoming air RH and used also Option 1. CEA and Quintessa applied the RH of incoming air (the same as JAEA), but used a flux boundary condition (Option 2) and predicted a RH on the tunnel wall somewhat higher than mean RH measured in the tunnel in agreement with the discontinuous RH profile along the air–rock interface. The approach used by CEA and Quintessa allowed them to predict the evolution of RH in the first rock centimetres (Fig. 19(b)). CAS and JAEA instead overestimated the decrease of RH in the first rock centimetres and the response to ventilation regime change was too pronounced, which is probably due to the direct application of the RH on the tunnel wall (Option 1).

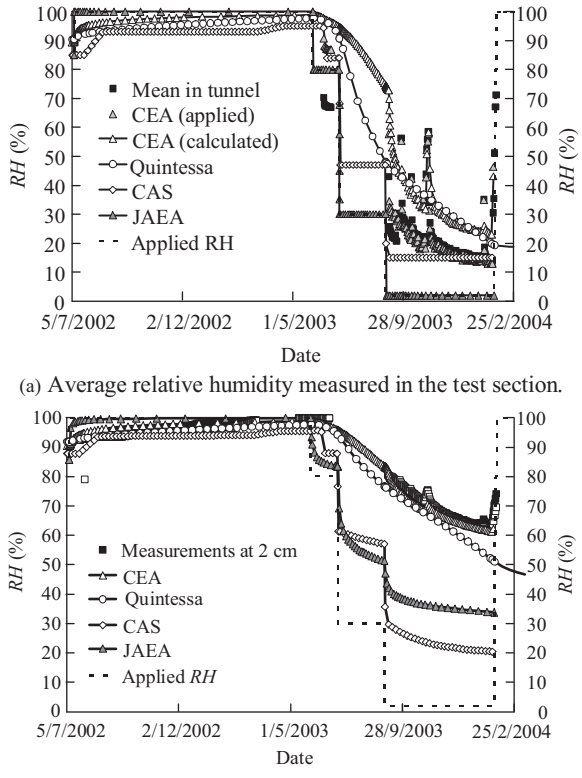

Fig. 19. Relative humidity in the tunnel and in the first rock centimetres.

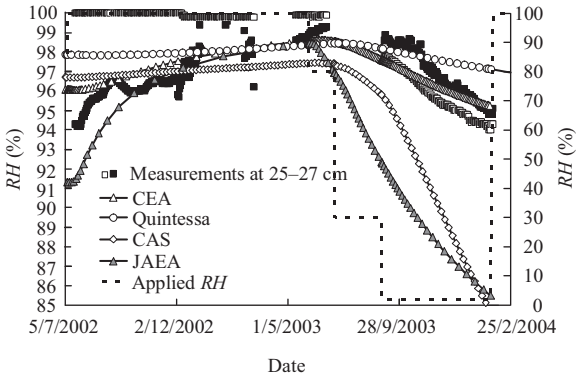

(a) Relative humidity 25 cm inside the rock mass.

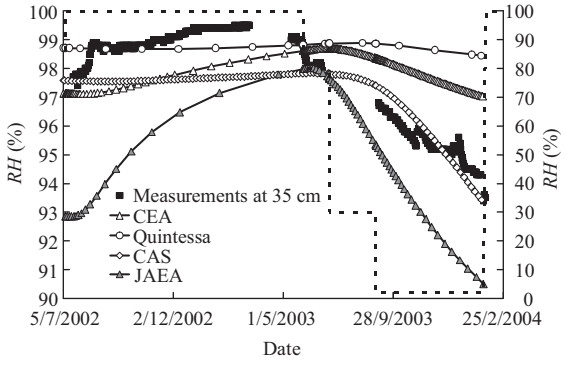

(b) Relative humidity 35 cm inside the rock mass.

Fig. 20. Measured and simulated relative humidity of various points inside the rock mass.

At 25 cm (Fig. 20(a)), the tendency of the measurements is also better reproduced by the teams considering the flux condition. The situation is reversed at 35 cm (Fig. 20(b)), although it should be noted that the measured values are very close to 100% and hence not totally reliable.

The measurements from the 24 piezometers are plotted in Fig. 21. Obviously, most of the piezometers do not monitor any response at all as before the start of the VE, all sensors closer to 1.8 m from the tunnel wall are situated in the suction zone. Those between 1.8 and 2.1 m from the wall exhibit an initial pore water pressure between 120 and 800 kPa. Once the drying phase starts, they respond quickly. Although the simulations predict quite well

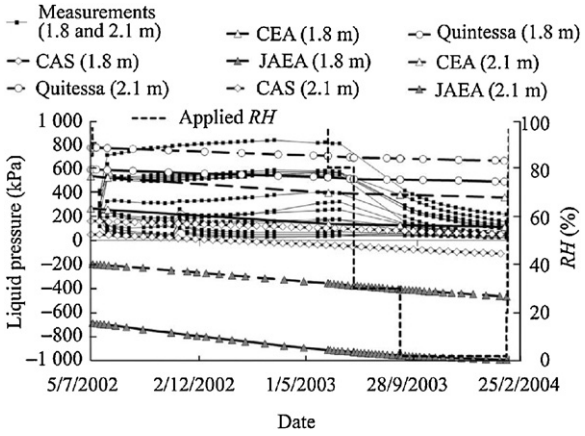

Fig. 21. Measured and simulated pore water pressure between 1.8 and 2.1 m from the microtunnel wall.

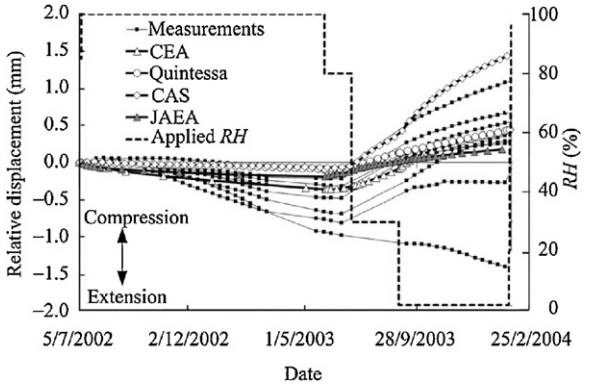

Fig. 22. Measured and simulated relative displacement between the microtunnel wall and points 2 m inside the rock mass.

the pore water pressure state before the drying phase, they do not succeed in reproducing the rapid pore water pressure drop when drying starts. This consistent failure to reproduce this phenomenon by all the teams suggests that some process in the modelling is missing. Given the rapidity of the pressure drop, we are inclined to believe that it is caused by some mechanical response of the rock to drying as hydraulic dissipation would involve a much longer response time.

Eight extensometers were installed in the test section. They show that wetting induces an expansion of the rock mass and drying a compression (Fig. 22). The simulations represent quite well the tendency that is explained by the changes in suction during the drying–wetting cycles that affect the effective stress. The strain changes induced by the wetting-drying cycles have a small amplitude compared to other processes like excavation.

The final state of the rock mass at the end of the first ventilation phase is summarized in Fig. 23. The extent of the suction zone has been enlarged (from 1.65–1.8 m before the VE to 1.8–2.1 m). There is a large scatter between the predicted suction limit from the different teams (1 m from the tunnel wall up to more than 3 m) although some of the teams succeeded to reproduce the measured profile quite well given the scatter of the data. The partial desaturation limit is not extended, but is strongly intensified. This tendency is well reproduced by the teams.

4.3. Advanced modelling of the VE

After the calibration of the first ventilation phase, minor changes in the parameters set were carried out and new modelling features were introduced. Perhaps, the most significant advance has been the development of models simulating the air flow in the tunnel allowing for prescribing the air flow and RH directly at the in-pipe. These new features were described in details in Bond et al. (2013a). Anisotropic material features were also introduced (Millard et al., 2013). Consideration of water permeability anisotropy explained the differences in water content profiles measured in the bedding plane direction and in perpendicular direction. It also provided a sensible explanation for the scatter observed in the RH and pore water pressure data. The rapid evolution of pore water pressure after ventilation regime changes was qualitatively explained by stiffness anisotropy although the magnitude of the pressure drop could not be reproduced. The largest changes in parameters were introduced by the teams that did not consider vapour diffusion. The influence of vapour diffusion was found less significant than that in the laboratory experiment. The reason is probably that in the in situ test, an inexhaustible water reservoir is available and desaturation is thus less intense than that in laboratory. This caused JAEA and

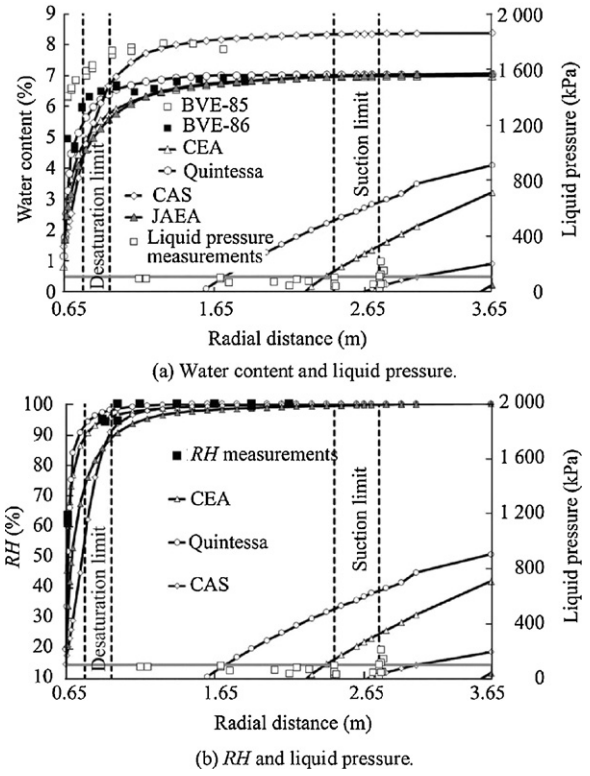

Fig. 23. Measured and simulated profiles of water content, relative humidity and pore water pressure at the end of the first ventilation period (26 January 2004).

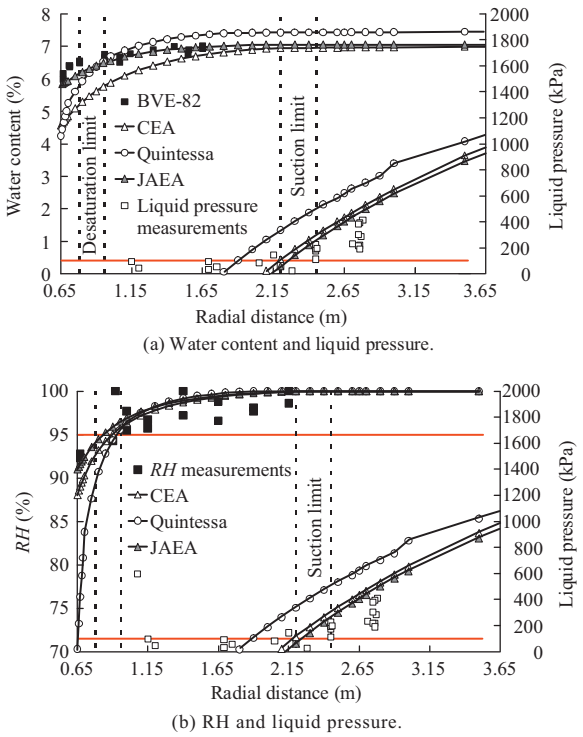

Fig. 24. Measured and simulated profiles of water content, relative humidity and pore water pressure just before the sealing of the test section (5 July 2002).

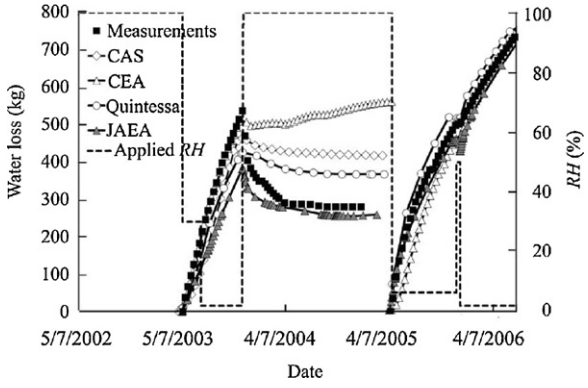

Fig. 25. Measured and simulated water mass balance of the test section.

UoE to adopt a permeability value and relative permeability much close to that employed by the teams considering vapour diffusion.

In Phase 1, RH in the rock mass was monitored by hygrometers concentrated between 30 cm up to 2.15 m from the tunnel wall. Before the experiment, the likely position of the saturation limit was estimated to be in that range, but it appeared to be overestimated. Indeed, in that range, all hygrometers provided readings above 95% which is above the confidence limit of these devices. After Phase 1, it was only possible to state that the partially desaturated zone extent was less than 30 cm from the tunnel wall. Four new hygrometers were installed in the first 30 cm before Phase 2. These hygrometers allowed for a better characterization of the RH gradient in Phase 2.

In terms of pore water pressure and determination of the suction limit, the opposite occurred. Most of the piezometers were installed in the suction zone whose extent was estimated to be much close to the desaturation limit before the test. In Phase 2, three new piezometers were installed from gallery 1998 in the farther field of the VE. This allowed a better characterization of the pore water pressure gradient.

The initial conditions before starting the VE are re-examined in Fig. 24. One of the improvements is the better reproduction of the suction limit by all the teams.

The water mass balance is plotted in Fig. 25 over the entire duration of the experiment. It has been reset to 0 at the start of the second phase for comparison purposes. The blind prediction of Phase 2 is almost perfect. JAEA used an improved version of Option 1 for the evaporation boundary condition. They still applied the RH directly, but they used an empirically determined value between the RH measured in the tunnel and that in the first rock centimetres. The calibration of the empirical relationship was done on the basis of Phase 1 and Phase 2 is thus purely predictive. Nevertheless, they still obtained an abrupt response to ventilation regime change. CAS instead changed their boundary condition to Option 2. Quintessa upgraded their model to Option 3 and hence the results are purely predictive. In other words, Quintessa may perform a pure blind prediction of a new VE without any in situ measurement of the new experiment. The RH they computed in the tunnel (Fig. 26) is an output of their modelling approach.

The RH evolution in the rock mass is presented in Fig. 27 at different distances from the tunnel wall. The measurements from the newly installed hygrometers in Fig. 27b–d which were not available to the teams during the project provided a good validation test.

Reproduction of pore water pressure evolution is only improved by teams that introduced stiffness anisotropy (CEA in Fig. 28). Although the improvement is only qualitative and the magnitude of the pore water pressure drop is not satisfactorily explained, the simulation carried out by CEA allows understanding the process generating the direct pore water pressure response to ventilation (Millard et al., 2013).

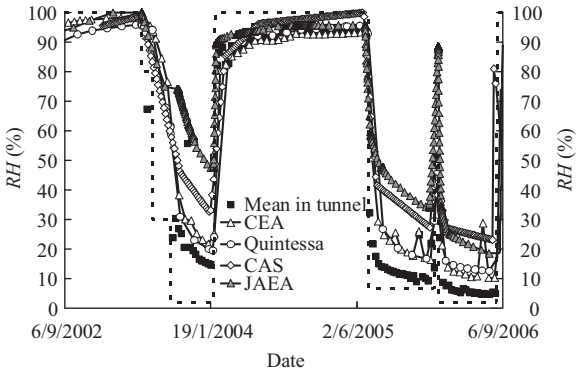

Fig. 26. Average relative humidity measured in the test section and calculated or applied relative humidity on the tunnel wall.

The compression–extension behaviour during drying–wetting cycles in the second phase is similar to the one observed in the first phase (Fig. 29). The measurements do not seem to indicate any accumulation of irreversible strains along the cycles although this should be confirmed in another experiment, considering shorter strain measurement intervals (2 m in the VE). Condensation of the ventilation system during the resaturation phase caused flooding of the microtunnel floor. This event seems to have induced an irreversible extension of the rock in the bottom of the microtunnel and even caused failure of one of the extensometers.

The rock state at the end of the first drying phase is summarized in Fig. 30. According to the measurements carried out in the drilling campaign at the end of the second resaturation phase and the RH measurements, the rock is fully saturated before the start of the second drying phase (Fig. 31). Although some of the farthest piezometers recovered during the resaturation phase, the suction limit did not change significantly. The simulation results

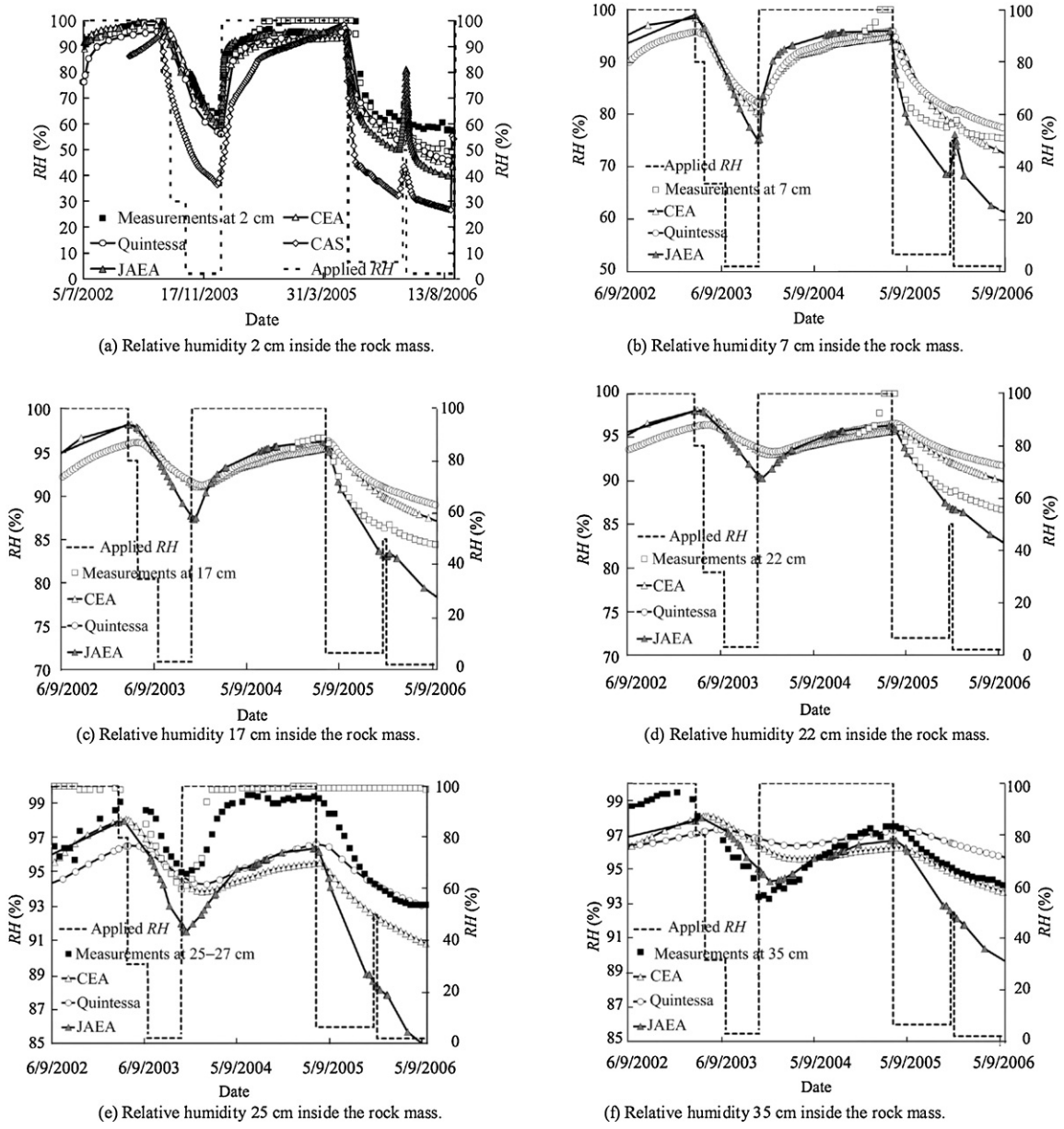

Fig. 27. Measured and simulated relative humidity of various points inside the rock mass (advanced modelling).

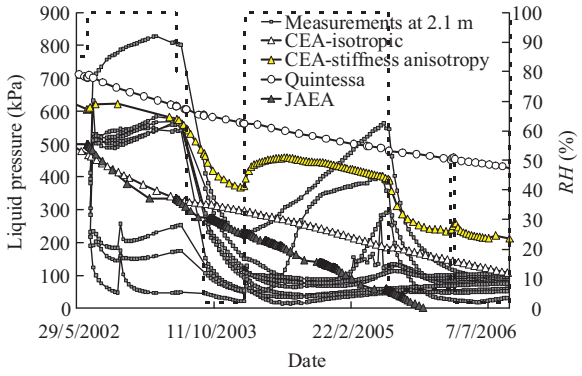

Fig. 28. Measured and simulated pore water pressure between 1.8 m and 2.1 m from the microtunnel wall.

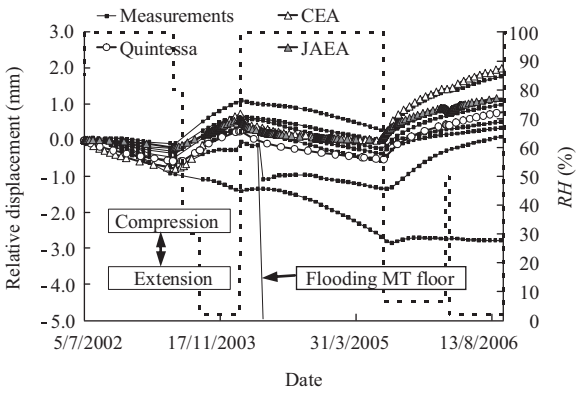

Fig. 29. Measured and simulated relative displacement between the microtunnel wall and points 2 m inside the rock mass.

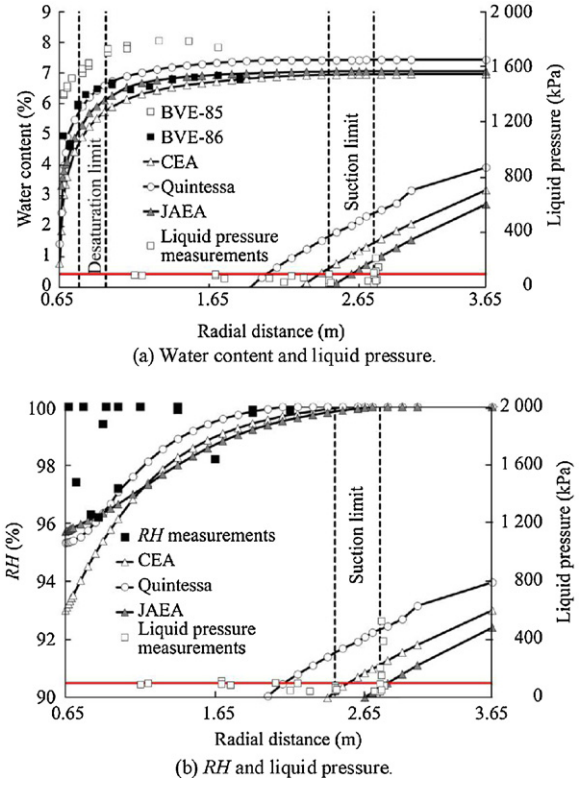

Fig. 30. Measured and simulated profiles of water content, relative humidity and pore water pressure at the end of the ventilation period (26 January 2004).

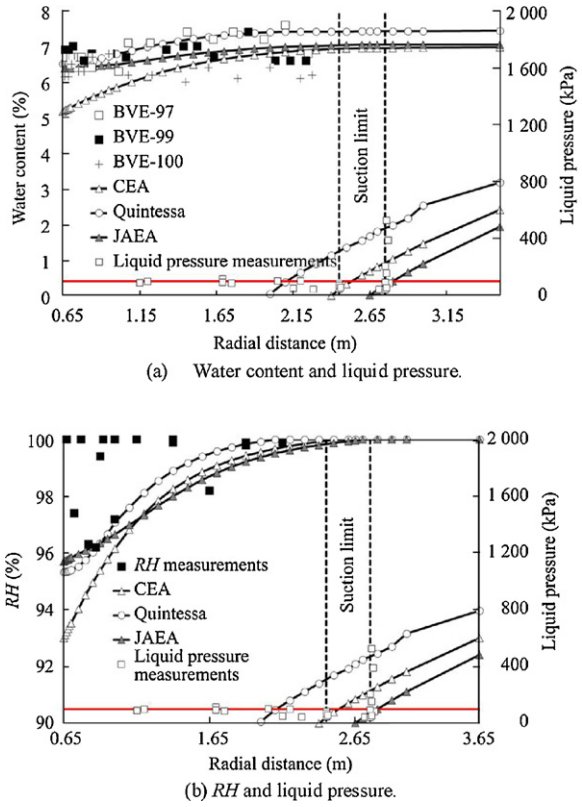

Fig. 31. Measured and simulated profiles of water content, relative humidity and pore water pressure at the start of the second resaturation period (1 May 2005).

reproduced adequately the saturation state before the start of the second drying phase.

From the water content and RH measurements, the partially desaturated zone seems to reach 25–30 cm into the tunnel wall at the end of Phase 2 (Fig. 32).

The measured profiles are quite well reproduced by the different teams. The new hygrometers allowed a more reliable characterization of the RH gradient. Boreholes BVE-104 and BVE-108 were drilled in the test section in the direction perpendicular to the bedding planes and in the bedding plane, respectively. Borehole BVE-111 was drilled between the test section and the tunnel end to evaluate the effect of a year-long closure on the saturation state. All piezometers installed before Phase 1 are in suction, which means that the suction limit is farther than 2.1 m inside the rock mass. The closest new piezometer registered a pore water pressure of about 600 kPa. The suction limit thus certainly does not extent further than 3.5 m, but is likely to be close to 2.1 m, given the high pore water pressure value registered at 3.5 m. The pore water pressure profiles predicted by the teams indicate somewhat higher pressure than the new piezometers. This is probably due to the fact that these piezometers are located in the middle area between the microtunnel and gallery 1998, which was not taken into account in the models.

The long-term evolution of the pore water pressure in the new piezometers is presented in Fig. 33 up to the end of 2010. The measurements exhibit a cyclic behaviour with local maximum each year in February. The cyclic behaviour is related to the temperature variation in gallery 1998 and to the propagation of the heat wave into the rock mass; temperature increases generate pore water pressure increases. Disregarding the thermal cycles, it is possible to state that the long-term prediction provided by the teams is satisfactory given the complexity of the test history and the fact that gallery 1998 has not been taken into account in the modelling.

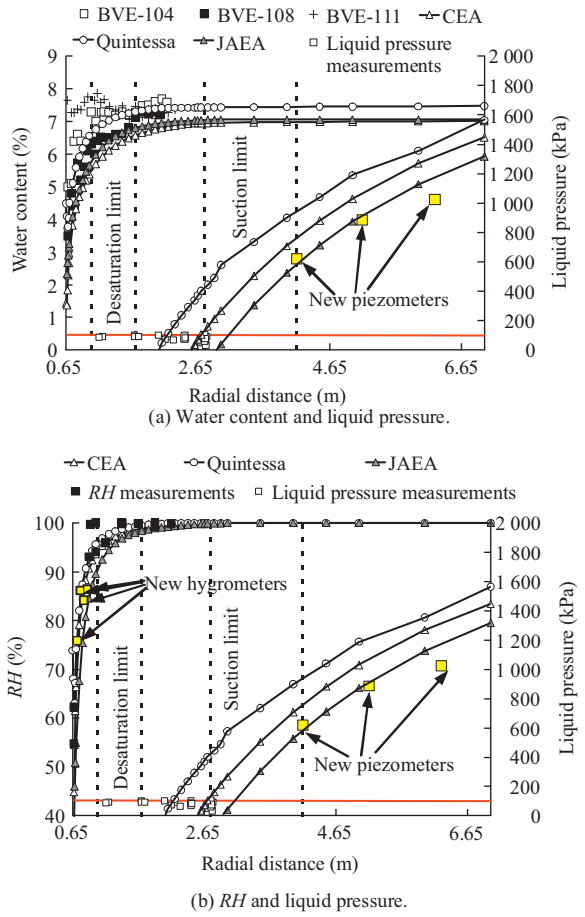

Fig. 32. Measured and simulated profiles of water content, relative humidity and pore water pressure at the end of the second ventilation period (4 October 2006).

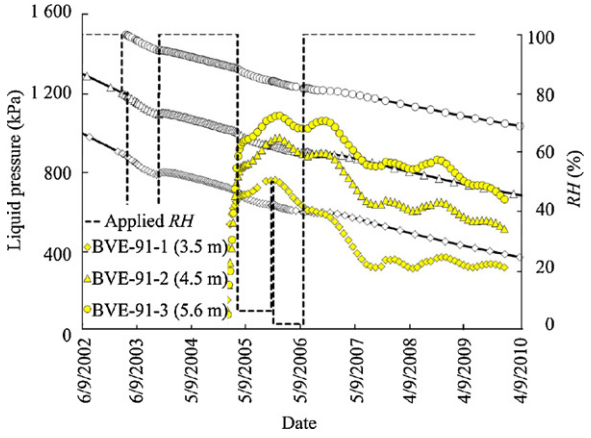

Fig. 33. Measured and simulated long-term evolution of pore water pressure between 3.5 and 5.6 m from the microtunnel wall. Simulation results are from CEA.

As a consequence of the marine origin of Opalinus clay, its pore water contains a significant amount of salt. In presence of water evaporation, salt concentration will happen. One of the complementary objectives of the VE was to evaluate the importance of this phenomenon. Comprehensive research has also been carried out on geochemistry processes in the framework of DECOVALEX 2011. Only the main findings are reported here as this is the subject of one of the companion papers (Bond et al., 2013b). First of all, chloride concentration increases were measured near the wall of the tunnel according to the different drying phases although no salt deposition occurred. The chloride gradient could be reproduced by the models using a one-solute transport model as chloride was believed to be a conservative (non-reactive) species. The possible influence of this gradient on the generation of an additional osmotic flow component was assessed and seemed to be totally negligible. Quintessa also run a fully reactive transport model to explain the higher sulphate/chloride concentration ratio in the unsaturated zone than in the saturated zone which indicates the occurrence of chemical reactions.

5. Summary of the identified mechanisms/processes

The analysis of the laboratory drying test and the in situ VE included the identification and discussion of all possible processes that may influence the test results and more particularly the rock behaviour. The modelling work carried out in this project enabled the relevance of a number of desaturation processes to be assessed. A hierarchical classification is proposed:

(1) Water transport occurs mainly through water pressure gradients and is thus determined by the permeability of the porous medium.
(2) In the unsaturated zone, vapour diffusion has a non-negligible influence. The importance of this process is less in the in situ test than in the laboratory drying test. This is because desaturation is less intense due to an inexhaustible amount of water available in the far field.
(3) A correct evaluation of the dependency of the water permeability on the saturation degree was found to be necessary.
(4) An accurate representation of the retention curve is necessary, because of its importance in the determination of the permeability of the partially unsaturated zone and of its influence on the boundary between the partial desaturation zone and the suction zone.
(5) Anisotropic rock properties (permeability and stiffness) were shown to explain some second order phenomena.
(6) Stress redistribution is suspected to have a possible influence on the permeability in the 10–20 cm close to the microtunnel. The good agreement between measurements and simulation results using a permeability value that does not vary with damage indicates that permeability increase in the EDZ may be neglected in experiments involving a similar diameter tunnel.
(7) The strains generated by the drying–wetting cycles themselves were very low and did not produce any significant change in porosity, which could have introduced a back influence on the transport problem.
(8) Osmotic flow was estimated to have little significance (0.01%–0.05% of classical Darcy flow).

6. Conclusions

The 4-year long controlled ventilation conditions applied to an unlined microtunnel have provided a set of important HM(C) observations. The interpretation of the experiment has been performed with the aid of several numerical tools. Most of the parameters were determined on the basis of a literature review and interpretation of laboratory tests (drying test and retention curve). This approach has allowed the calibration of a number of important rock parameters. The simulations achieved close quantitative agreement with the experiment in many instances and showed their ability to explain qualitatively most observations.

Heavy ventilation conditions applied during 1–2 years were found to produce a partially desaturated zone of quite a limited

extent, much smaller than those thought initially. The limit of the partially desaturated zone was estimated to 25–30 cm and the suction limit was about 2 m (or even somewhat more) after a ventilation period of 20 months. The difference between suction and partial desaturation limit has been attributed to the retention behaviour of Opalinus clay.

The VE may be regarded as a huge pump test and may thus be used to determine the hydraulic conductivity of Opalinus clay. Common agreement between the modelling teams seems to indicate an intrinsic permeability value of about 10^{-19} m^2 for saturated rock. This value lies in the upper range of many measurements carried out at Mont Terri but fits quite well the measurements done in the piezometers of the VE area. The models used led to a very satisfactory reproduction of an important quantity of measurements (water mass balance of the experiment, the relative humidity, pore water pressure, water content and deformation). The consistent results between the different codes and the measurements are an important validation of the numerical tools.

Acknowledgements

The work described in this paper was conducted within the context of the international DECOVALEX Project. The authors are grateful to the Funding Organizations who supported the work. The views expressed in the paper are, however, those of the authors and are not necessarily those of the Funding Organizations. The data used in this work were obtained in the framework of the EC project NF-PRO (Contract number FI6W-CT-2003-02389) under the coordination of ENRESA (Empresa Nacional de Residuos Radiactivos).

References

Bock H. RA experiment rock mechanics analyses and synthesis: data report on rock mechanics. Mont Terri Project: Technical Report 2000-02. Ittigen, Switzerland: Federal Office for Water and Geology (FOWG); 2001.

Bond A, Millard A, Nakama S, Zhang C, Garitte B. Approaches for representing hydro-mechanical coupling between large engineered voids and argillaceous porous media at ventilation experiment, Mont Terri. Journal of Rock Mechanics and Geotechnical Engineering 2013a; 5 (2); in press.

Bond A, Benbow S, Wilson J, Millard A, Nakama S, English M, et al. Reactive and non-reactive transport modelling in partially water saturated argillaceous porous media around the ventilation experiment, Mont-Terri. Journal of Rock Mechanics and Geotechnical Engineering 2013b;5(1):44–57.

Bossart P, Meier PM, Moeri A, Trick T, Mayor JC. Geological and hydraulic characterisation of the excavation disturbed zone in the Opalinus clay of the Mont Terri rock laboratory. Engineering Geology 2002;66(1/2):19–38.

Brooks RH, Corey AT. Properties of porous media affecting fluid flow. Journal of the Irrigation and Drainage Division, ASCE 1966;92(2):61–90.

Chijimatsu M, Fujita T, Kobayashi A, Nakano M. Calibration and validation of thermal, hydraulic and mechanical model for buffer material. Tokai, Japan: JNC Technical Report, JNC TW8400 98-017; 1998.

Fernández AM, Melón A, Turrero MJ, Villar MV. Geochemical characterisation of the rock samples for the VE-Test before a second cycle of drying. Ventilation test phase II. Madrid: CIEMAT; 2006.

Floría E, Sanz FJ, García-Siñeriz JL. Drying test: evaporation rate from core samples of "Opalinus clay" under controlled environmental conditions. Madrid: AITEMIN; 2002.

Garitte B, Gens A. The response of an argillaceous rock to ventilation: process identification and analysis of an in situ experiment. In: Qian QH, Zhou YX, editors. Harmonizing rock engineering and the environment, Proceedings of the 12th ISRM international congress on rock mechanics. London: Taylor and Francis Group; 2011. p. 634–5.

Garitte B, Gens A, Liu Q, Liu X, Millard A, Bond A, et al. A DECOVALEX-2011 benchmark: laboratory drying test in Opalinus clay. In: EC-TIMODAZ-THERESA THMC Conference. Luxemburg: European Commission; 2009.

Garitte B, Gens A, Liu Q, Liu X, Millard A, Bond A, et al. Modelling benchmark of a laboratory drying test in Opalinus Clay. In: Rock Mechanics in Civil and Environmental Engineering. London: Taylor and Francis Group; 2010. p. 767–70.

Gens A. HE experiment: complementary rock laboratory tests. Mont Terri Project: Technical Note TN 2000-47; 2000.

Gens A, Vaunat J, Garitte B, Wileveau Y. In-situ behaviour of a stiff layered clay subject to thermal loading: observations and interpretation. Geotechnique 2007;57(2):207–28.

Gisi M. Evaporation logging FM-D experiment: modification of the equipment. Mont Terri Project: Technical Note 2007-27; 2007.

Ippisch O, Vogel HJ, Bastian P. Validity limits for the van Genuchten–Mualem model and implications for parameter estimation and numerical simulation. Advances in Water Resources 2006;29(12):1780–9.

Martin CD, Lanyon GW. Measurement of in situ stress in weak rocks at Mont Terri Rock Laboratory, Switzerland. International Journal of Rock Mechanics and Mining Sciences 2003;40(7/8):1077–88.

Maul PR. The Quintessa Multiphysics General-Purpose Code QPAC. Warrington, UK: Quintessa Ltd; 2010.

Mayor JC, Velasco M. The ventilation experiment phase II (synthesis report). NFPRO Project W.P.4.3; 2008.

Meier E. FM-D experiment: evaporation logging in the new gallery. Mont Terri Project: Technical Note 98-51; 1998.

Meier E. Evaporation logging (FM-D) experiment, Phase 9: documentation of raw and processed data. Mont Terri Project: Technical Note 2004-50; 2004.

Millard A, Bond A, Nakama S, Zhang C, Barnichon JD, Garitte B. Accounting for anisotropic effects in the prediction of the hydro-mechanical response of a ventilated tunnel in an argillaceous rock. Journal of Rock Mechanics and Geotechnical Engineering 2013; 5 (2); in press.

Muñoz JJ, Lloret A, Alonso E. Characterization of hydraulic properties under saturated and non-saturated conditions. NFPRO Project Deliverable 4 EC Contract FIKW-CT2001-00126; 2003.

Nussbaum C, Bossart P. Compilation of *K*-values from packer tests in the Mont Terri rock laboratory. Mont Terri Project: Technical Note 2005-10; 2004.

Schaeren G, Norbert J. Tunnel du Mont Terri et du Mont Russelin. La traversée des roches à risques: marnes et marnes à anhydrite, SIA-Dokumentation D037, La traversée du Jura – Les projets des nouveaux tunnels. Zürich: Swiss Society of Engineers and Architects (SIA); 1989.

Schuster K. Ventilation test (VE) experiment: final activity report on high resolution seismic investigations within the VE-Experiment. Mont Terri Project: Technical Report 2007-06; 2007.

Thury M, Bossart P. The Mont Terri rock laboratory, a new international research project in a Mesozoic shale formation, in Switzerland. Engineering Geology 1999;52(3/4):347–59.

Traber D. Geochemical characterisation of samples from drill core BVE82. NFPRO Project Deliverable D5b EC Contract FIKW-CT2001-00126; 2003.

Traber D. Geochemical characterisation of samples from drill core BVE85 and BVE86. NFPRO Project Deliverable D5c&d/D22 EC Contract FIKW-CT2001-00126; 2004.

Verpeaux P, Millard A, Charras T, Combescure A. A modern approach of large computer codes for structural analysis. In: Hadjian AH, editor. ProcSMiRT. Los Angeles: AASMiRT; 1989. p. 75–85.

Villar MV. Retention curves determined on samples taken before the second drying phase. CIEMAT Technical Report M2144/5/07; 2007.

Wermeille S, Bossart P. In situ stresses in the Mont Terri Region: data compilation. Mont Terri Project: Technical Report 99-02; 1999.

Wileveau Y. THM behaviour of host rock (HE-D) experiment: progress report (Part 1). Mont Terri Project: Technical Report TR 2005-03; 2005.

Zhang CL, Rothfuchs T. Report on instrument layout and pre-testing of large lab VE-tests. NFPRO Deliverable 4.3.11; 2005.